Felix Rosenthal\*, Tobias Pahl, Tim Eckhardt, Marco Künne, and Peter Lehmann

# Concept and application of the three-dimensional transfer function in optical surface topography measurement

Konzept und Anwendung der dreidimensionalen Transferfunktion zur optischen Oberflächentopografiemessung

https://doi.org/10.1515/teme-2025-0057

Abstract: The concept of the three-dimensional optical transfer function (3D-TF) has become an increasingly important tool in understanding and modeling the measurement behavior of modern optical surface metrology systems, particularly in the context of coherence scanning interferometry (CSI). The 3D-TF enables a comprehensive description of how spatial frequency components, both lateral and axial, of electromagnetic fields are transmitted through the optical system. This opens up a wide range of applications: from fast simulation of the measurement processes to enhanced signal analysis and surface reconstruction techniques, and to the full characterization and calibration of measurement systems. In this paper we describe our attempts to determine the 3D-TF, which was already calculated analytically, also in practice.

**Keywords:** Optical transfer function; Coherence scanning interferometry; surface topography measurement; modeling

Zusammenfassung: Das Konzept der dreidimensionalen optischen Transferfunktion (3D-TF) ist zu einem wichtigen Werkzeug für das Verständnis und die Modellierung des Messverhaltens moderner optischer Oberflächenmesssysteme geworden, insbesondere im Zusammenhang mit der Kohärenz-Scanning-Interferometrie (CSI). Die 3D-TF ermöglicht eine umfassende Beschreibung, wie räumliche Frequenzkomponenten – sowohl lateral als auch axial – von elektromagnetischen Feldern durch das optische System übertragen werden. Dies eröffnet eine Vielzahl von Anwendungsmöglichkeiten: von der schnellen Simulation der Messprozesse über verbesserte Signalanalyse- und Oberflächenrekonstruktionsverfahren bis hin zur vollständigen Charakterisierung und Kalibrierung von Messsystemen. In

diesem Beitrag beschreiben wir unsere Versuche, die bereits analytisch berechnete 3D-TF auch experimentell anhand von Messdaten zu bestimmen.

Schlagwörter: Optische Übertragungsfunktion; Kohärenz-Scanning-Interferometrie; Messung der Oberflächentopografie; Modellierung

#### 1 Introduction

Optical measurement instruments are widely used for fast and contactless surface topography inspection with applications in science as well as industry. Coherence scanning interferometry (CSI) [1, 2], also known as white light interferometry, is one of the most common techniques to analyze micro- and even sub-micrometer surface features and stands out due to its extraordinary axial and diffraction-limited lateral resolution. Like all optical measurement techniques, CSI suffers from diffraction effects, aberrations, misalignment etc. causing systematic measurement errors.

In order to understand the mechanisms behind these errors, several simulation models have been developed in the last decade [3–12], which differ with respect to accuracy, computation time and physical insight into the measurement process and thus in their applicability. Recently, progress has been made in the modeling of CSI instruments considering the imaging process by a three-dimensional transfer function (3D-TF) in the 3D spatial frequency domain [7, 8, 13, 14]. Especially the derivation of an analytical expression of the 3D-TF [14, 15] allows fast simulations with the so-called universal Fourier optics (UFO) model [9].

In addition, the 3D-TF significantly contributes to an improved understanding of the measurement process, which, for instance, is used to optimize signal processing [14, 16, 17], analyze misalignment effects [18, 19], compensate for aberration errors [20], and calibrate measurement instruments [21]. Although the 3D-TF is meanwhile a well-known concept, its accurate determination is still challenging. In

<sup>\*</sup>Corresponding author: Felix Rosenthal, Measurement Technology, Department of Electrical Engineering and Computer Science, University of Kassel, Wilhelmshöher Allee 71, 34121 Kassel, E-Mail: f.rosenthal@uni-kassel.de 00009-0009-3167-9136

this context, it should be noted that the 3D-TF is based on a theoretical concept for infinitely small point scatterers, which scatter light homogeneously in the pupil plane of the microscope objective lens [15]. However, infinitely small point scatterers are typically not apparent in reality and are hard to find with regard to technical surfaces. First attempts have been made to obtain the 3D-TF practically by measuring spheres of a certain radius [20, 21]. However, the scattering characteristics of spheres with large radii compared to the wavelength of light differ from the assumed concept of a point scatterer [22]. Moreover, producing appropriate spheres of small radius with the required surface smoothness is extremely challenging. Note that in addition to concepts of 3D-TFs based on point scatterers, specular surfaces are also considered [14].

This study deals with different approaches to obtain the 3D transfer function for CSI instruments from measurement data. The concepts are presented theoretically using FEM-based simulations. Basically, three different concepts are presented and discussed: measuring a diffraction grating, tilting a plane mirror, and measuring a sphere.

## 2 Concept of the optical 3D transfer function

Three-dimensional transfer functions generally provide a comprehensive description of the transfer behavior of optical surface topography measuring instruments in the spatial frequency domain. Figure 1 presents the general shape and values of an exemplary 3D-TF, where Fig. 1a) shows how wave vectors  $\mathbf{k}_{in}$  of the incident and  $\mathbf{k}_{s}$  of the scattered light wave form the  $\mathbf{q}$ -space according to

$$\mathbf{q} = \mathbf{k}_{s} - \mathbf{k}_{in} \,. \tag{1}$$

The construction of the 3D-TF is based on Ewald spheres, which provide a geometric framework for visualization of all possible combinations of incident and scattered wave vectors according to the numerical aperture of the system [23]. The red solid lines in Fig. 1a) show the limits of the transfer function for in-plane scattering. The upper limit is given by back-scattering with  $\mathbf{k}_{\rm S} = -\mathbf{k}_{\rm in}$ , which results in  $\mathbf{q} = 2\mathbf{k}_{\rm in}$ . The maximum value of  $q_{z,\rm max} = 2k_0$ , with wave number  $k_0 = 2\pi/\lambda_0$  and light wavelength  $\lambda$ , is reached at  $q_x = q_y = 0$ , the maximum value of  $q_{x,\rm max} = 2k_0 \mathrm{NA}$  at  $q_{z,\rm min} = 2k_0 \sqrt{1-\mathrm{NA}^2}$ . The red dashed line indicates the lower limit of the transfer function. The area enclosed by the dashed line and the bows of the solid lines corresponds to out-of-plane scattering. The 3D-TF can also be calculated analytically. This is illustrated in Fig. 1b), which shows a

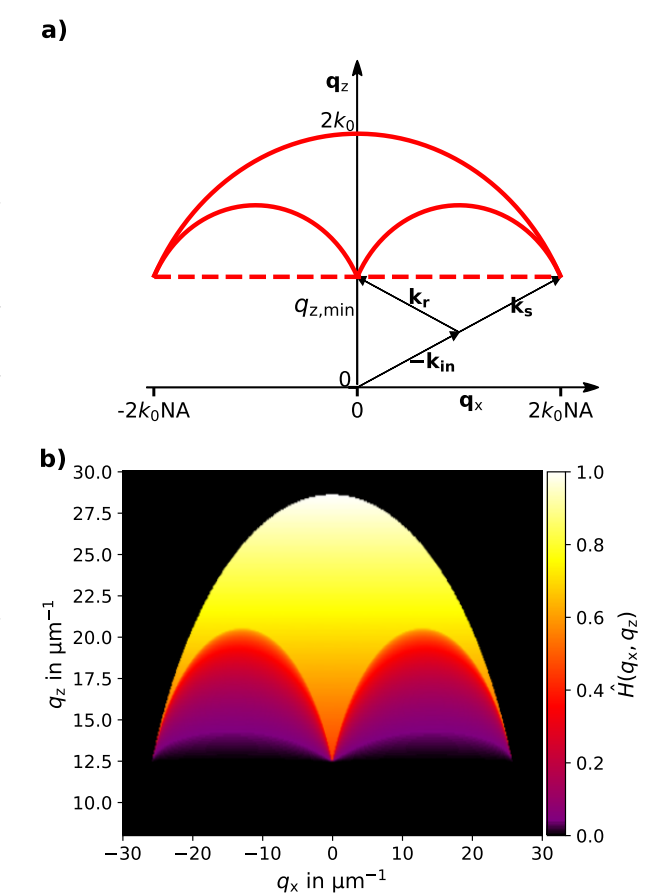


Fig. 1: a) Construction of the Ewald limiting sphere defining the q-space, b) 2D cross section in the  $q_x$ ,  $q_z$ -plane of the monochromatic 3D-TF of a microscope of NA = 0.9 for the wavelength  $\lambda=440\,\mathrm{nm}$ .

2D cross section of the normalized 3D-TF  $\hat{H}(q_x,q_z)$  in the  $q_x$ ,  $q_z$ -plane for a numerical aperture of NA = 0.9 and a wavelength of  $\lambda = 440\,\mathrm{nm}$ . The analytical expression for this transfer function is derived in detail in [14]. For further information on the derivation and the underlying physical assumptions, we also refer to this work.

## 3 Practical determination of the 3D transfer function

As mentioned above, a measuring device can be described by its associated 3D-TF. For its experimental determination it is necessary that the examined objects evoke spatial frequencies in the same area in frequency space that is covered by the expected TF. This can be achieved by diffraction or scattering of the measuring surface. In addition, the intensity distribution in this region should be as homogeneous as possible.

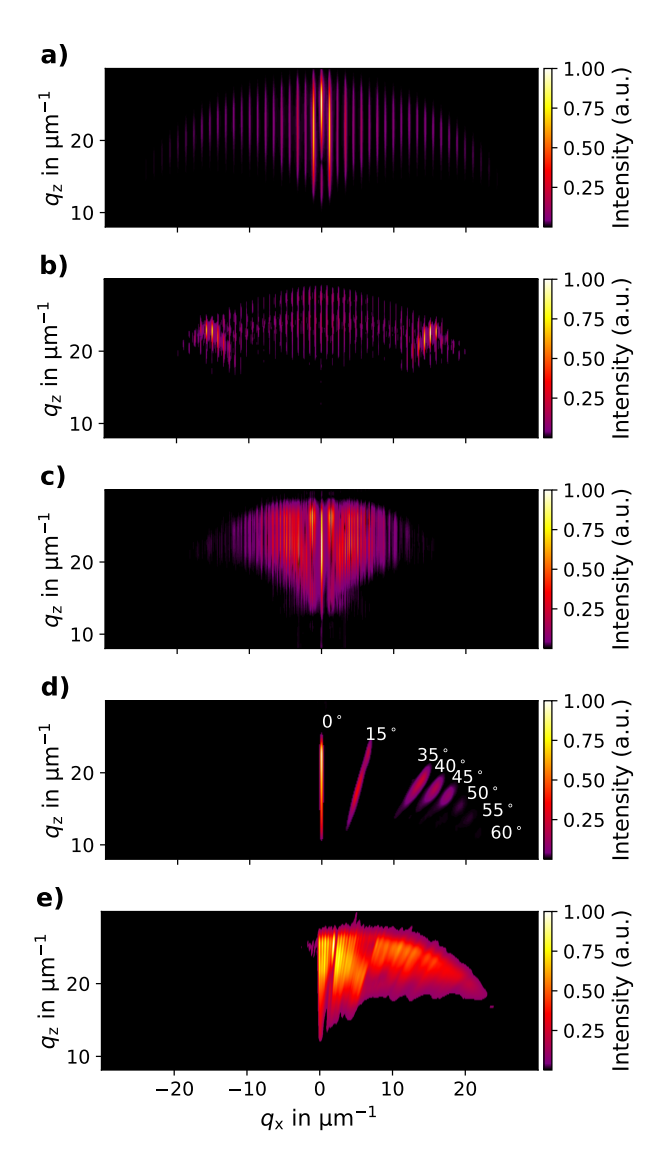


Fig. 2: Slices in the  $q_x$ ,  $q_z$ –plane of Fourier transformed image stacks of different objects measured with a Linnik interferometer with an NA = 0.9. a) rectangular reflection grating of  $6~\mu m$  period length, b) triangular reflection of  $8~\mu m$  period, c) PTB chirp standard, d) plane metal mirrors adjusted at different discrete tilt angles and e) plane metal mirror continuously tilted and readjusted.

A Linnik interferometer [24, 25] with an NA of 0.9 and a light source with an central wavelength of  $\lambda_c=440\,\mathrm{nm}$  and a full width at half maximum (FWHM) of 20 nm was used as an exemplary measuring instrument. Various measurement objects were examined, their image stacks recorded, and the corresponding 3D Fourier transforms determined. The results can then be understood as a product of the scattered

field of the measurement objects and the 3D-TF of the measurement device in the spatial frequency domain. In the following, we compare several ways of reconstructing the 3D-TF. One option is to obtain the transfer function with as many scattering orders of a grating as possible. This can be achieved with gratings with long period lengths where at the same time several periods (approx. 10) are in the field of view of the system. With the Linnik interferomter used here, this can be realized with grating periods in the range of 5 µm to 15 µm. Measurements were carried out with a rectangular grating with a period length of 6 µm (RSN [26]) and a triangular grating with a period length of 8 µm (Gr-P 8-35t [27]). The corresponding intensity distributions in Fourier space are shown in Figs. 2a) and 2b). The corresponding diffraction orders can be recognized for both gratings and are well distributed in the region of the optical transfer function. With both measurements, however, there is the problem that there is a concentration of intensity at certain locations. For the rectangular grating structure, this can be seen around the zeroth diffraction order of the grating, while for the triangular grating it appears at higher orders, corresponding to the slope angles of the surface flanks of app. 35°. Other slope angles of the flanks would, therefore. lead to other intensity concentrations (this observation is also exploited later for further results). These extremely uneven distributions of intensity in the different diffraction orders lead to problems in the further evaluation or analysis of these measurement series. In Sec. 4, we show an approach in which a sinusoidal grating is simulated, which provides a more homogeneous distribution. In addition to lattice structures with a fixed period length, a PTB chirp standard [28] was also measured. The basic idea here is that the range of the TF can be well estimated, due to different spatial frequencies of the individual sinusoidal surface sections. Figure 2c) shows that this only works for smaller spatial frequencies and that there are small gaps in the spectrum. Higher orders or generally higher frequency components that enable to determine the edges of the 3D-TF are hardly available.

Next, plane mirrors were measured, which are tilted by angles of 0°, 15°, 35°, 40°, 45°, 50°, 55°, 60°. The measurements were carried out consecutively. Fourier transformed image stacks were summed up and the resulting image is shown in Fig. 2d). For the angle of 0° the signal of a plane mirror is obtained. If the mirror is tilted, a similar signal appears, but tilted by the angle in frequency space. If this is repeated for many angles up to the maximum angle related to the NA, the region of the expected TF can be sampled. The concept of Fig. 2d) was repeated for a larger number of tilt angles as shown in Fig. 2e). This leads directly to the problem with this method: Due to the high number of indi-

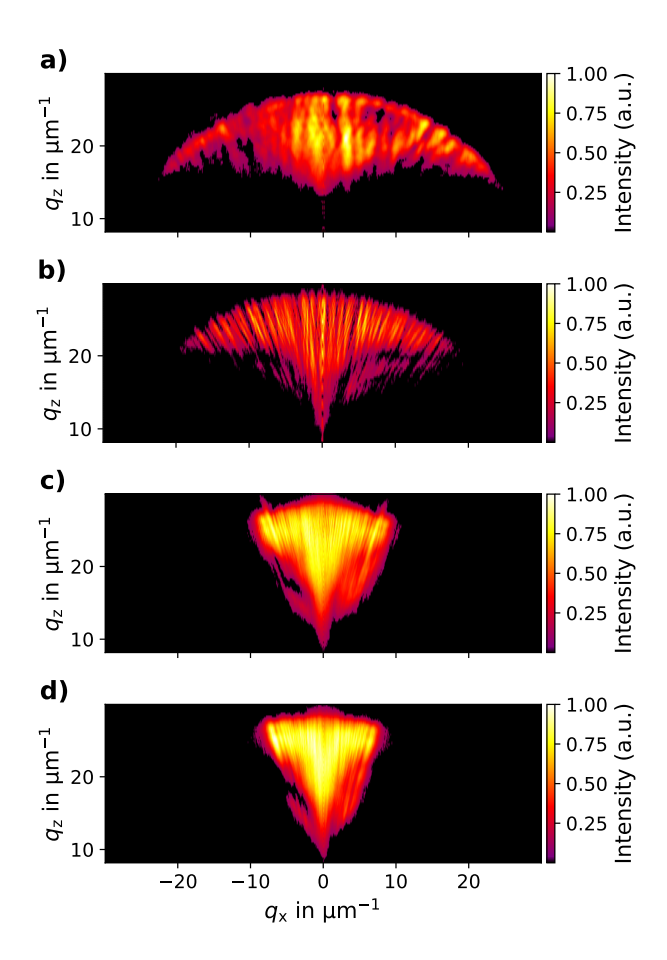


Fig. 3: Slices in the  $q_x$ ,  $q_z$ -plane of Fourier transformed image stacks of different objects measured with a Linnik interferometer of NA = 0.9. a) Steel microsphere ( $6\,\mu\mathrm{m}$  diameter), ruby sphere with b)  $120\,\mu\mathrm{m}$  diameter, c)  $250\,\mu\mathrm{m}$  diameter, and d)  $300\,\mu\mathrm{m}$  diameter, respectively.

vidual measurements, the procedure is very time consuming, which makes it difficult to maintain the same measurement conditions for all measurements. In this experiment, small misalignments occurred, which can be recognized by the discontinuities in the image shown. Due to this, the approach is rather inappropriate for determining the TF.

Investigations were also carried out on spherical surfaces of high curvature. When illuminating reflecting spheres or half-spheres with infinitely small radii, it can be assumed that they behave like point scatterers. These provide the advantage that, by definition, the intensity distribution is constant over all scattering angles. The larger the radius of surface curvature, the less they behave like a point scatterer. Figure 3 shows Fourier transformed image stacks of measurements of different spheres: a) steel sphere of 6  $\mu$ m diameter, b), c), and d) ruby spheres of 120  $\mu$ m, 250  $\mu$ m, and 300  $\mu$ m) diameter, respectively. The steel microsphere, Fig. 3 a), initially shows a good sampling of all frequency

components in the region of the expected 3D-TF. However, it is also clear that this region does not have a homogeneous intensity distribution. Some scattering angles seem to contribute less than others. This is due to the rough surface of the sphere. The ruby sphere with a diameter of 120 µm, Fig. 3 b), shows a similar behavior. Here, it can be assumed that the spheres do not have a perfect surface, too. Likewise, higher  $q_x$  frequency components, which were recognizable for the steel microsphere, no longer appear. This is because larger surface inclination angles are required for higher spatial frequency components. Although these are generally present on the sphere's surface, they can no longer be recorded by the measuring device due to its limited field of view. This effect also occurs for spheres with even larger radii (see Fig. 3 c) and d)). The maximum achievable scattering angle therefore becomes smaller. For the larger ruby spheres, however, a better homogeneity of the scattering field can be seen, which, in comparison to before, speaks for more smooth and homogeneous surfaces. In theory, spheres are sufficient to determine the TF via an analysis in Fourier space. These must be as small as possible  $d_{\rm sphere} \leq 40\,\mu{\rm m}$  and at the same time, they should be manufactured as perfect as possible. However, even if this were achieved, the small amount of scattered light is a problem. Therefore, in the next section a method will be presented, which theoretically makes it possible to determine the 3D-TF experimentally.

## 4 Determination the 3D transfer function based on sinusoidal surfaces

In recent sections, approaches are introduced with the aim of reconstructing the optical 3D-TF from measured data. These include the use of diffraction gratings, microspheres, and tilted planar mirrors, each offering distinct advantages and challenges in terms of spatial frequency coverage and signal interpretation. While these measurements provide valuable insights, they are inherently affected by the complex scattering behavior of real objects and potential experimental impacts such as alignment errors or signal distortions. To overcome these limitations and to gain a deeper understanding of the underlying principles, the following section focuses on a theoretical investigation of the optical 3D transfer function. The focus here will again be on grating structures. Note that even for a sinusoidal phase grating multiple diffraction orders occur. As shown before, we need gratings with period lengths of  $5\,\mu m$  to  $15\,\mu m$  to

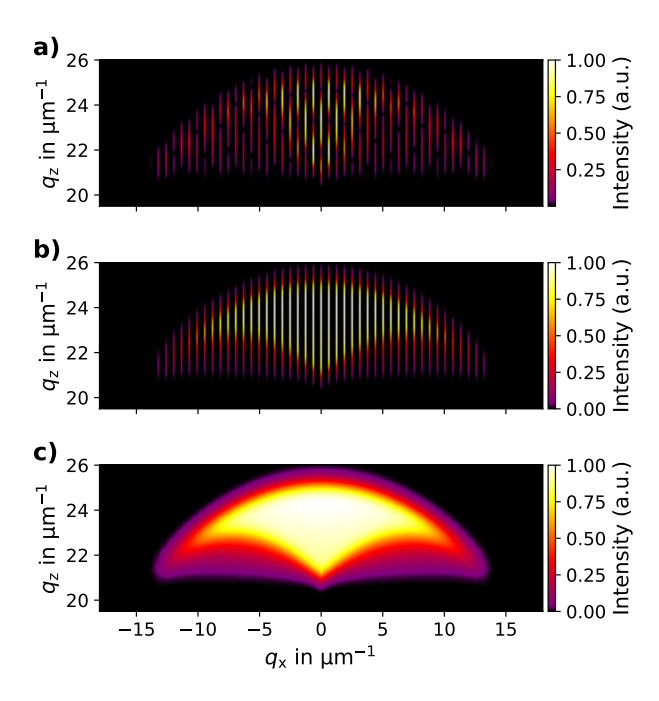


Fig. 4: a) Slices in the  $q_x$ ,  $q_z$ -plane of the Fourier-transformed image stack of a simulated sine standard, b) transfer function at the discrete diffraction orders, c) complete transfer function calculated by interpolation between the diffraction orders.

get a good coverage of the spatial frequencies in the range of the expected TF. With respect to the gratings already investigated, it was found that the intensity distribution of different diffraction orders is not homogeneous. This can be changed by choosing the right grating structure. Figure 4a) shows an FEM simulation [6] for a sinusoidal reflection grating with a period length of 10 µm and a peak-to-valley amplitude (PV) of 2.23 µm. The CSI instrument is characterized by NA = 0.55, a mean wavelength of  $550 \, \text{nm}$ , and a FWHM of 10 nm. The amplitude of the sinusoidal surface is selected in order to achieve a maximum slope angle of 35° of the sinusoidal slope, which matches the maximum possible capture angle of a Mirau objective with NA = 0.55. This configuration was chosen since steep slope angles of sinusoidal surfaces are difficult to be produced, but 35° is still within the accessible range. When considering the intensity changes between the individual diffraction orders, it is noticeable that these are significantly more homogeneous for this approach, thus making it easier to extract the transfer function. For the determination of the 3D-TF, the scattering field of the sinusoidal surface is determined via FEM simulation. This allows the 3D-TF to be determined at the  $q_x$  positions of the different diffraction orders by dividing the Fourier transformed image stack at these positions by the corresponding scattered field. The result is shown in Fig. 4b). The complete transfer function can

now be determined by interpolating the calculated sections along the  $q_x$ -axis (Fig. 4c)).

### 5 Conclusion

In this work, we present the concept of the three-dimensional optical transfer function (3D-TF) and discuss its relevance for modeling and analyzing modern state-of-the-art topography measurement systems, particularly in the context of coherence scanning interferometry. We examine various experimental approaches to determine the 3D-TF from measured data. These include the use of diffraction gratings, tilted planar mirrors, and spherical surfaces of high curvature. For each of these methods specific limitations, such as inhomogeneous intensity distributions, restricted spatial frequency coverage, or practical challenges in sample fabrication and alignment, are highlighted. To overcome these issues, we propose an approach based on the simulated scattered field of a sinusoidal phase grating. This method allows us to approximate the transfer function more uniformly by dividing the measured data by the precomputed scattered field at individual diffraction orders. While this approach has shown promising results, it remains a theoretical investigation at the moment. Future work will focus on validating this method experimentally to enable a reliable reconstruction of the 3D transfer function from real measurements.

**Acknowledgment:** The authors gratefully acknowledge the financial support of the following research project (Grant No: LE 992/18-1) by the Deutsche Forschungsgemeinschaft (DFG).

#### References

- J. Schmit, K. Creath, and J.C. Wyant. "Surface profilers, multiple wavelength, and white light interferometry". In: *Optical Shop Testing*. Ed. by Daniel Malacara. New York: Wiley, 2007, pp. 667–755.
- [2] Peter de Groot. "Coherence scanning interferometry". In: Optical Measurement of Surface Topography. Ed. by Richard Leach. Berlin, Heidelberg: Springer, 2011, pp. 187– 208.
- [3] Peter J. de Groot and Xavier Colonna de Lega. "Fourier optics modeling of interference microscopes". In: *Journal of* the Optical Society of America A 37.9 (2020), B1–B10.
- [4] Peter de Groot et al. "Modeling of coherence scanning interferometry using classical Fourier optics". In: Optical Engineering 60.10 (2021), p. 104106.

- Matthew Thomas et al. "Modeling of interference mi-[5] croscopy beyond the linear regime". In: Optical Engineering 59.3 (2020), pp. 034110-034110.
- T. Pahl et al. "3D modeling of coherence scanning interferometry on 2D surfaces using FEM". In: Optics Express 28.26 (2020), pp. 39807-39826.
- Rong Su et al. "Scattering and three-dimensional imaging [7] in surface topography measuring interference microscopy". In: Journal of the Optical Society of America A 38.2 (2021), A27-A42.
- Rong Su and Richard Leach. "Physics-based virtual coherence scanning interferometer for surface measurement". In: Light: Advanced Manufacturing 2.2 (2021), pp. 120-135.
- Peter Lehmann, Tobias Pahl, and Jörg Riebeling. "Universal Fourier optics model for virtual coherence scanning interferometers". In: Proc. SPIE 12619 (2023), 1261900.
- Tobias Pahl et al. "Electromagnetic modeling of interference, confocal, and focus variation microscopy". In: Advanced Photonics Nexus 3.1 (2024), p. 016013.
- Helia Hooshmand et al. "Comparison of Fourier opticsbased methods for modeling coherence scanning interferometry". In: Optical Engineering 63.4 (2024), p. 044102.
- Tobias Pahl et al. "Rigorous full 3D modeling of coherence scanning interferometry and confocal microscopy". In: Journal of Physics: Photonics 7.3 (2025), p. 035011.
- Jeremy M. Coupland and J. Lobera. "Holography, tomography and 3D microscopy as linear filtering operations". In: Measurement science and technology 19.7 (2008), p. 074012.
- P. Lehmann, S. Hagemeier, and T. Pahl. "Threedimensional transfer functions of interference microscopes". In: Metrology 1.2 (2021), pp. 122-141.
- [15] Peter Lehmann and Tobias Pahl. "Three-dimensional transfer function of optical microscopes in reflection mode". In: Journal of microscopy 284.1 (2021), pp. 45-55.
- Peter Lehmann, Marco Künne, and Tobias Pahl. "Analysis of interference microscopy in the spatial frequency domain". In: Journal of Physics: Photonics 3.1 (2021), p. 014006.
- Peter Lehmann et al. "Analysis and improvement of the lateral resolution of CSI instruments based on the universal Fourier optics (UFO) model". In: Proc. SPIE 12997 (2024),
- Rong Su et al. "Effects of defocus on the transfer function of coherence scanning interferometry". In: Optics Letters 43.1 (2017), pp. 82-85.
- Tim Czasch et al. "Extension of the 3D analytical transfer function for coherence scanning interferometry". In: Measurement 253 (2025), p. 117617.
- Rong Su et al. "Lens aberration compensation in interference microscopy". In: Optics and Lasers in Engineering 128 (2020), p. 106015.
- Rong Su et al. "On tilt and curvature dependent errors and [21] the calibration of coherence scanning interferometry". In: Optics Express 25.4 (2017), pp. 3297–3310.
- Hendrik C. van de Hulst. Light scattering by small particles. New York: Dover Publications, Inc., 1981.
- [23] Max Born and Emil Wolf. Principles of optics: electromagnetic theory of propagation, interference and diffraction of light. Elsevier, 2013.

- Weichang Xie et al. "Signal modeling in low coherence interference microscopy on example of rectangular grating". In: Optics express 24.13 (2016), pp. 14283-14300.
- [25] Sebastian Hagemeier. "Comparison and investigation of various topography sensors using a multisensor measuring system". PhD thesis. Kassel, Universität Kassel, 2022.
- [26] Simetrics. http://www.simetrics.de/pdf/RS-N.pdf. accessed June 08, 2025.
- Simetrics. http://www.simetrics.de/pdf/Gr-P.pdf. accessed [27] June 08, 2025.
- [28] Uwe Brand et al. "Sensors and calibration standards for precise hardness and topography measurements in microand nanotechnology". In: Micro-Nano-Integration; 6. GMM-Workshop. VDE. 2016, pp. 1-5.